Available online at www.sciencedirect.com
ScienceDirect
Polymer 48 (2007) 6415–6425
polymer
www.elsevier.com/locate/polymer

PVDF porous matrix with controlled microstructure prepared by TIPS process as polymer electrolyte for lithium ion battery

Gen-Liang Ji, Bao-Ku Zhu, Zhen-Yu Cui, Chun-Fang Zhang, You-Yi Xu*

Department of Polymer Science and Engineering, Zhejiang University, Hangzhou 310027, China

Received 13 June 2007; received in revised form 5 August 2007; accepted 15 August 2007
Available online 23 August 2007

Abstract

Poly(vinylidene fluoride) (PVDF) microporous matrix of polymer electrolyte for lithium ion battery was prepared via the thermally induced phase separation (TIPS) process using diluent mixture of dibutyl phthalate (DBP) and di(2-ethylhexyl) phthalate (DEHP). Since this method has only one parameter, namely the DBP/DEHP ratio in diluent mixture, the membrane microstructure is easily and conveniently controlled. With the assistance of a pseudo-binary temperature-DBP ratio phase diagram of the PVDF-diluent mixture system, the membrane formation mechanism for different microstructures of membranes was proposed. In addition to studying the different microstructures available in TIPS process, the relationship between performance of membrane, electrochemical property of polymer electrolyte and final microstructure has been investigated in this paper.
© 2007 Elsevier Ltd. All rights reserved.

Keywords: Thermally induced phase separation; Membrane microstructure; Polymer electrolyte

1. Introduction

Poly(vinylidene fluoride) has shown high potential to be used as the polymer matrix of polymer electrolyte for applications in rechargeable batteries [1–8]. The most recent research activity in the field of PVDF gel electrolyte has shown that good results can be obtained by the phase inversion technique [4–8]. It is possible to obtain conductivity as high as 10^{-3} S/cm at room temperature, while maintaining outstanding mechanical properties. Highly porous PVDF membranes have been extensively prepared by Bellcore's technology (air-casting of a polymer solution) [4,5], modified Bellcore's technology [6,7], and immersion precipitation technology [8]. By using these methods, it is able to obtain membranes with different structures, such as ''cell-like'' structure, ''finger-like'' structure and ''sponge-like'' structure. However, there are many complicated parameters to be controlled for obtaining the membranes with controlled structure in these methods. In the process of Bellcore's technology, the microstructure of membrane is controlled by the evaporation condition and the interaction of polymer–solvent and solvent–nonsolvent. On the other hand, conventional immersion precipitation technology is a more complicated process due to the effects of temperature, the interaction of polymer–solvent and the exchange condition between solvent and nonsolvent on the formation of membrane structure.

A few studies have been reported on preparation of PVDF microporous membrane via thermally induced phase separation (TIPS) method [9–13]. The well-documented advantage of TIPS method is the ease of control compared to conventional casting process [14,15]. The TIPS process begins by dissolving a polymer in a diluent at an elevated temperature. The solution is then cast or extruded into the desired shape (flat sheet, hollow fiber, etc.) and cooled to induce phase separation and polymer solidification (crystallization or glass transition). The diluent is extracted by solvent exchange and the extractant is usually evaporated to yield a microporous structure. When thermal energy is removed from a homogeneous polymer–diluent mixture, the TIPS can occur via solid–liquid (S–L) or

* Corresponding author. Tel./fax: +86 571 87953011.
E-mail address: opl-yyxu@zju.edu.cn (Y.-Y. Xu).

0032-3861/$ - see front matter © 2007 Elsevier Ltd. All rights reserved.
doi:10.1016/j.polymer.2007.08.049

liquid–liquid (L–L) phase separation depending on the polymer–diluent interaction, the composition and the thermal driving force. In previous studies, only spherulitic structures of PVDF membranes prepared by PVDF/single diluent systems via TIPS process were obtained. In order to obtain various structures of membranes prepared via TIPS process, several modified TIPS technologies were investigated, such as the thermally assisted evaporative phase separation (TAEPS) [16] and the combined use of thermally induced phase separation and immersion precipitation [17]. Although novel membrane microstructures were created, these new processes had a large number of parameters to control the membrane structures. Recently, preparation of membrane by using diluent mixture via TIPS process shows good results in controlling membrane structure. The structures of membranes based on EVOH, PLGA, PE and HDPE matrixes have been controlled systematically by using diluent mixture to control the polymer–diluent interaction [18–21].

In this study, polymer electrolytes based on PVDF microporous matrix were prepared by phase inversion technique. PVDF porous membranes were prepared along with diluent mixtures (dibutyl phthalate (DBP)/di(2-ethylhexyl) phthalate (DEHP)) via the TIPS method. The objective of this study is to demonstrate the effect of the interaction between diluent and polymer on the structure of membrane, and to control the structure of membrane systematically by varying the composition of diluent mixture. The effects of membrane structure on the performance of membrane and polymer electrolyte were also discussed.

2. Experimental

2.1. Materials

The PVDF ($M_n = 5.73 \times 10^5$, $M_w/M_n = 1.7$) used in the study was provided by Solvay Solexis (1015). DBP and DEHP, supplied by Guangdong Guanghua Chemical Regent Co., Ltd and Shanghai Chemical Reagent Co., Ltd, respectively, were used for preparing diluent mixtures without further purification. Both DBP (b.p. 340 °C) and DEHP (b.p. 386 °C) have boiling points much higher than the melting point of PVDF (174 °C) and they are miscible with each other. Viscosity, density and Hansen solubility parameters for PVDF and diluents are listed in Table 1.

2.2. Preparation of the PVDF/DBP/DEHP blend sample

Homogeneous diluent mixtures (DBP/DEHP) of known concentration were prepared beforehand. Since PVDF hardly dissolves in pure DEHP at higher temperature (240 °C), the diluent mixtures with the ratio of DBP/DEHP over 28 wt/72 wt, in which PVDF dissolves more quickly to form homogeneous solution at 240 °C, were chosen as the latent diluents for this study. PVDF and the diluents were mixed at an elevated temperature (240 °C) under nitrogen atmosphere for at least 3 h in a glass vessel with a stirrer. Then the glass vessel was quenched in liquid nitrogen to solidify the sample, and broken open to obtain the solid polymer–diluent sample. Homogeneous solid samples of 30 wt% PVDF with diluent mixtures of various DBP/DEHP ratios were prepared.

Table 1
Viscosity, density and Hansen solubility parameters for PVDF and diluents

Substance	Viscosity (mPa s (20 °C))[a]	Density (g/cm^3)[a]	δ_d (MPa$^{1/2}$)[a]	δ_p (MPa$^{1/2}$)[a]	δ_h (MPa$^{1/2}$)[a]
DBP	163	1.045	17.8	8.6	4.1
DEHP	80	0.985	16.6	7	3.1
PVDF	–	1.780	17.2	12.5	9.2

[a] Ref. [22].

2.3. Determination of the phase diagram

The cloud point (T_{cloud}), crystallization temperature (T_c) and melting temperature (T_m) were measured according to the method reported by Matsuyama et al. [17]. The solid sample was placed between a pair of microscope cover slips and a Teflon film with a circle opening in the center was inserted between the cover slips to prevent diluent loss by evaporation. The sample was heated on a hot stage (Linkam THMS600) to 240 °C at 10 °C/min and held for 1 min, then cooled to 40 °C at a rate of 10 °C/min. T_{cloud} was determined visually by the appearance of turbidity under an optical microscope (Nikon eclipse E600 POL). A DSC (Perkin–Elmer DSC-7) was used to determine the T_c and T_m. The solid sample was sealed in an aluminum differential scanning calorimetry pan, melted at 240 °C for 5 min to erase thermal history and cooled to 40 °C at 10 °C/min, and then heated to 240 °C at 10 °C/min again. The onset temperatures of the exothermic peak during the cooling and the endothermic peak during the heating were taken as T_c and T_m, respectively.

2.4. Preparation of the porous membrane and polymer electrolyte

Homogeneous polymer–diluent samples were placed on a stainless steel mould (Fig. 1). Vacuum silicone grease was applied to the edge of the upper cover slip to prevent diluent loss by evaporation. The samples were heated at 240 °C for 5 min on the heater and were pressed to films. And then the mould containing the film was taken out to quench in the water bath (25 °C) for 10 min. The diluent in the film was extracted by immersing in ethanol for 24 h. The final membranes were dried under vacuum at 50 °C for 24 h. These membranes were named as M-d28, M-d29, M-d30, M-d32.5, M-d35, M-d40, M-d50 and M-d100 according to the diluent mixture used (28/72, 29/71, 30/70, 32.5/67.5, 35/65, 40/60, 50/50, 100/0 wt/wt DBP/DEHP, respectively). The thickness of the membrane was adjusted by the mould to be 200 ± 2 μm as shown in Fig. 1.

The membranes were activated in a glove box by immersing in liquid electrolyte for 4 h to form polymer electrolytes. The liquid electrolyte consists of a 1 M solution of $LiPF_6$ in a 1 wt/1 wt/1 wt dimethyl carbonate/ethyl methyl carbonate/ethyl carbonate (DMC/EMC/EC) mixture. Conductivity of this liquid electrolyte is 10.4×10^{-3} S/cm.

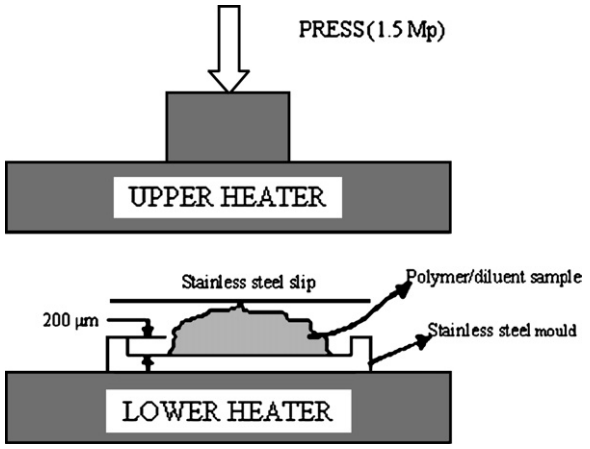

Fig. 1. Schematic diagram of hot-press apparatus for membrane preparation.

2.5. Characterization of the porous membrane

The dry membranes were freeze-fractured in liquid nitrogen and then sputter-coated (Hitachi® E1020) with gold. The cross-sections and the surfaces of the membranes were observed by a field-emitting SEM (Sirion-100, FEI Co., Netherlands).

The thermal stability and the crystallinity of PVDF membrane were studied using differential scanning calorimeter (DSC, Perkin–Elmer). The heating rate is 10 °C/min, the temperature range is from 50 to 200 °C. The crystallinity of PVDF membrane was calculated using the following equation:

$$X_c = \Delta H_f / \Delta H_f^0 \times 100\% \quad (1)$$

where X_c means the crystallintity of PVDF membrane, ΔH_f represents the fusion enthalpy of PVDF membrane. ΔH_f^0 is the fusion enthalpy of PVDF with 100% crystallinity which was previously reported to be 104.7 J/g [23].

Mechanical strength of membrane was conducted using an Instron testing machine (AG-1 electron pull equipment, Japan). The tensile rate was 25 mm/min. The tested specimens were 1 cm wide and 5 cm long.

The pore size distribution and porosity of membrane were evaluated using a mercury injection apparatus (Auto Pore IV9500, Micromeritics).

The liquid electrolyte uptake of membrane was calculated by the following equation:

$$\text{Electrolyte uptake} = \left(\frac{W_i - W_0}{W_i}\right) \times 100\% \quad (2)$$

Where W_0 is the mass of dry membrane, W_i is the weight of polymer electrolyte after absorbing the liquid electrolyte.

2.6. Characterization of the polymer electrolyte

The ionic conductivity of the polymer electrolyte was measured with the AC complex impedance technique over the frequency range from 0.1 Hz to 1 MHz, using a Solartron SI 1255B frequency response analyzer combined with an SI 1287 electrochemical interface. The polymer electrolytes for measuring the ionic conductivity were sandwiched between two stainless steel (SS) blocking electrodes as described previously [24]. The constant potential is 10 mV and the temperature range is 0–80 °C. Bulk resistance was obtained from measured AC impedance. Ionic conductivity was calculated by the equation below:

$$\sigma(\text{ionic conductivity}) = t/(R_b A) \quad (3)$$

where t is the thickness of polymer electrolyte, R_b, the bulk resistance of polymer electrolyte, and A is the area of polymer electrolyte.

The electrochemical stability window of the polymer electrolyte was determined by linear sweep voltammetry on an SS working electrode with lithium foil as the counter electrode, the scanning rate was 5 mv/s.

3. Results and discussion

3.1. Phase diagram

As described in Section 2, the phase separation behavior of PVDF/DBP/DEHP ternary systems was observed under optical microscope. When the DBP/DEHP ratio increased in the diluent mixture, the type of phase separation changed from the liquid–liquid phase separation to solid–liquid phase separation. Fig. 2 exhibits the changes in the morphology of blends as the DBP/DEHP ratio increased from 30 wt/70 wt to 40 wt/60 wt when the crystallization of PVDF in blend is completed. When the DBP/DEHP ratio was 30 wt/70 wt in diluent mixture, the observation revealed that liquid droplets started to nucleate and grow and finally were fixed in the spherulites of PVDF during cooling from 240 °C as shown in Fig. 2(a). On the other hand, the system with 40 wt/60 wt showed no evidence for L–L phase separation and only spherulite growth was observed during the cooling as shown in Fig. 2(b).

The diagram of 30 wt% PVDF samples prepared with several diluent mixtures of different DBP/DEHP ratios is shown in Fig. 3. As seen in Fig. 3, T_{cloud} decreased significantly with the increased DBP content in the diluent mixture, while T_c and T_m decreased slowly. When the DBP/DEHP ratio in diluent mixtures increased and reached 35 wt/65 wt, L–L phase separation was no longer observed experimentally, and only the polymer crystallization process was present.

The overall feature in Fig. 3 is analyzed in terms of the interaction between PVDF and the diluent mixture and the viscosity of systems. The estimated interaction parameter χ^*, typically used to interpret the interaction between the polymer and the diluent, was estimated from the difference of the solubility parameters between the polymer and the diluent using the following expression [25]:

$$\chi^* = \frac{V_m}{RT}\left[[\delta_{d1} - \delta_{d2}]^2 + [\delta_{p1} - \delta_{p2}]^2 + [\delta_{h1} - \delta_{h2}]^2\right] \quad (4)$$

where V_m is the reference volume which is equal to the molar volume of the specific repeating unit size of the polymer, δ_d and δ_p are the dispersive and the polar term of the solubility

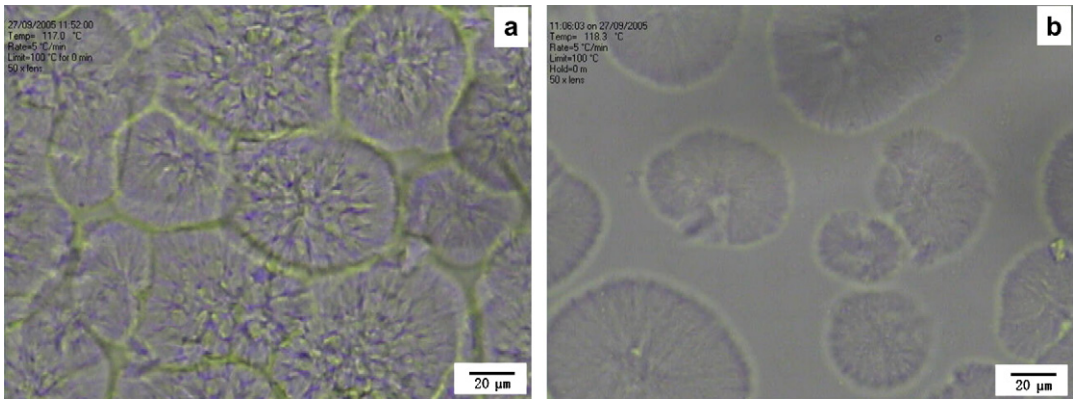

Fig. 2. Microphotographs for the system with 30 wt/70 wt DBP/DEHP (a) and for the system with 40 wt/60 wt DBP/DEHP (b), cooled to 100 °C from 240 °C at 10 °C/min.

parameter, respectively. δ_h is the hydrogen-bonding contribution to the solubility parameter, and 1 and 2 refer to the diluent and the polymer. By assuming that V_m is the same for every system, the interaction between PVDF and diluent for blends at a certain temperature and the same polymer concentration may be compared by molar excess free energy of mixing ΔG^E [22]:

$$\Delta G^E = [\delta_{d1}-\delta_{d2}]^2+[\delta_{p1}-\delta_{p2}]^2+[\delta_{h1}-\delta_{h2}]^2 \quad (5)$$

Smaller value of χ^* and ΔG^E presents better interaction between PVDF and the diluent. Subsequently, the value of solubility parameter for mixed diluent can be calculated by the following expression:

$$\delta_i = \delta_{i1}\Phi_1 + \delta_{i2}\Phi_2 \quad (6)$$

where Φ_1 is the volume fraction of one diluent, Φ_2 is the volume fraction of another diluent and i represents d, p and h. By combining Eqs. (2) and (3) with the values of parameters for PVDF and diluent in Table 1, ΔG^E can be determined as a function of the DBP/DEHP ratio in diluent mixture. Plotting ΔG^E against the DBP/DEHP ratio in diluent mixture gave a straight line, as shown in Fig. 4. Simultaneously, it was clear that the value of ΔG^E was decreasing proportionally with the increase of DBP/DEHP ratio in the diluent mixture, which expressed that the increase of DBP/DEHP ratio in diluent mixture enhanced the interaction between polymer and diluent mixture. As a result, the L–L phase separation happens before the crystallization as shown in Fig. 2, owing to the poor interaction between polymer and diluent. As the interaction further enhanced, there was no more L–L phase separation appearing but only crystallization of polymer (S–L phase separation). On the other hand, since DBP possesses higher viscosity than that of DEHP as shown in Table 1, the viscosity of system increased with the increase in DBP content. Higher viscosity and stronger interaction between PVDF and the diluent mixture lead to lower mobility of polymer segments and thus prevented crystal nucleation and growth of PVDF as DBP content increased. As a result, the system needed deeper degree of super cooling to form the crystal nuclei of PVDF and the crystallization temperature decreased as DBP content increased.

3.2. The microstructure of porous membranes

The evolution in the microstructure of the membrane prepared via thermally induced phase separation process depends on the thermodynamic factors and the kinetic factors [26].

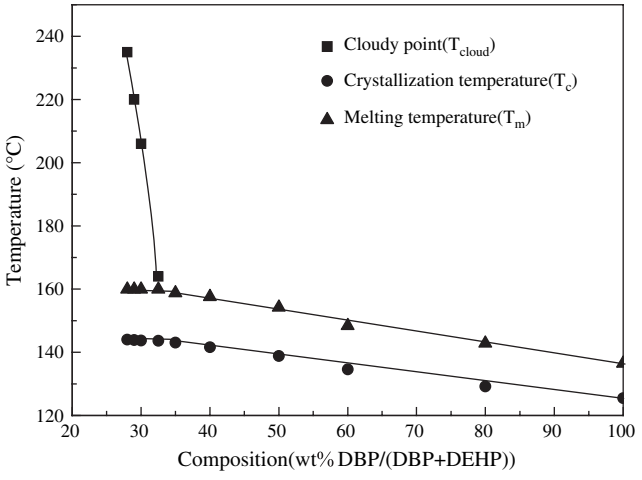

Fig. 3. Phase diagram of 30 wt% PVDF samples prepared with several diluent mixtures of different DBP content.

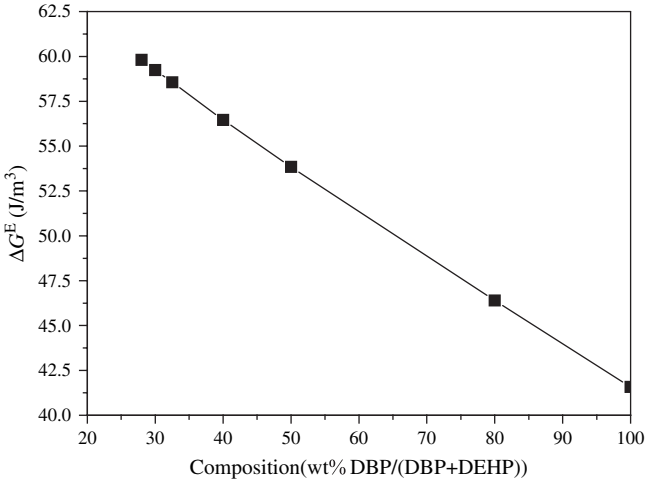

Fig. 4. Relation between DBP content in diluent mixture and molar excess free energy of mixing (ΔG^E).

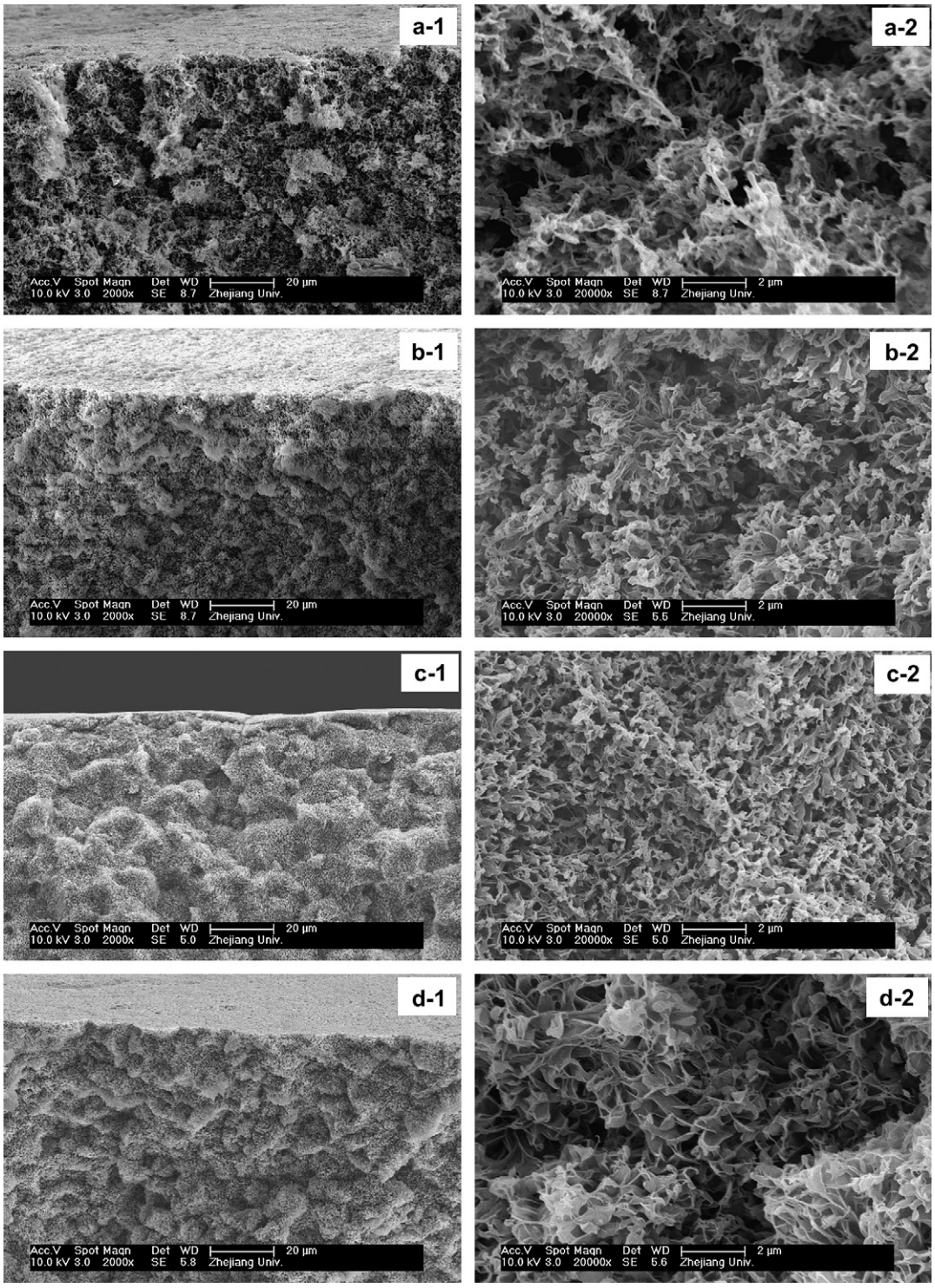

Fig. 5. SEM photographs of the cross-sections of 30 wt% PVDF membranes prepared via L–L phase separation. (a) M-d28, (b) M-d29, (c) M-d30, (d) M-d32.5. The bars represent 20 μm (1) and 2 μm (2) scales.

When the interaction between polymer and diluent is poor, the system must enter an unstable or a metastable region at the early cooling stage and undergoes the liquid–liquid phase separation. The phase separation proceeds through the nucleation and growth in the metastable region, while the spinodal decomposition occurs in the unstable region. After two phases, namely rich-polymer phase and lean-polymer phase, appear at the early stage of the microstructure development, the system will continue to evolve in response to its tendency to reduce the surface energy associated with interfacial area. The so-called coarsening process often results in the reduction in the number of droplets and an increase in their droplet size [27]. When the interaction between polymer and diluent is enhanced, the L–L phase separation shifts below the S–L phase, as was

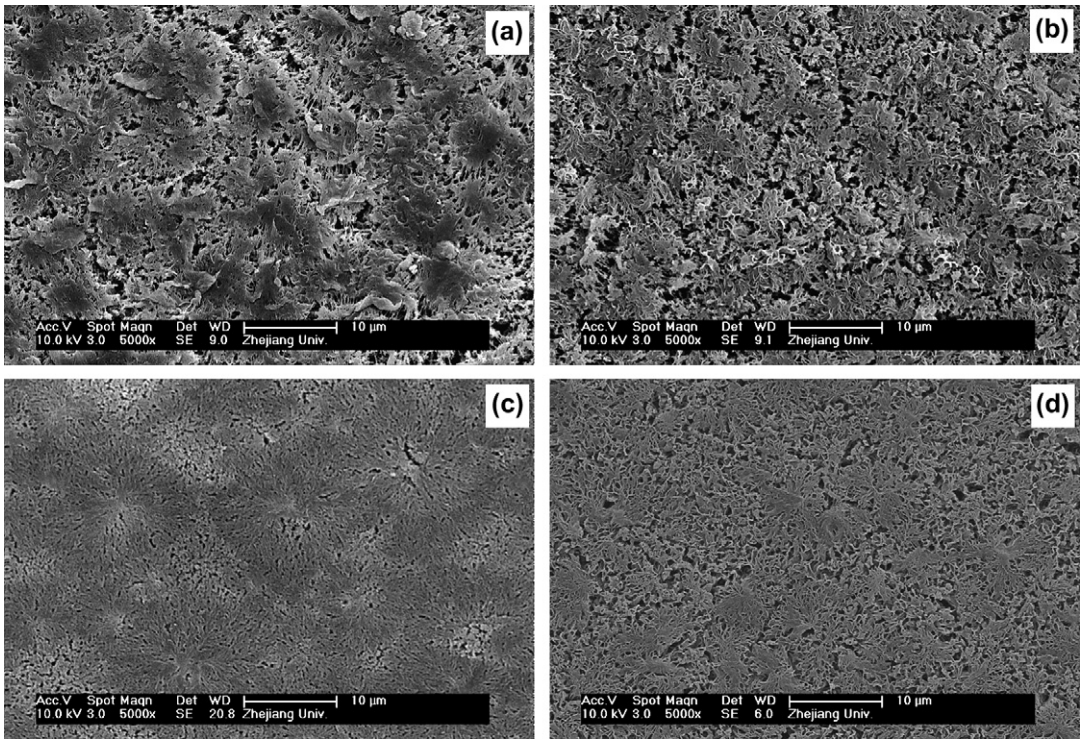

Fig. 6. SEM photographs of the surfaces of 30 wt% PVDF membranes prepared via L–L phase separation. (a) M-d28, (b) M-d29, (c) M-d30, (d) M-d32.5. The bars represent 10 μm scale.

predicted by Burghardt [28], and cannot be observed before crystallization. And only the crystal structure can be observed and controlled by varying cooling rate, polymer concentration and the interaction between polymer and diluent [29].

For the conditions where the liquid–liquid phase separation was observed before crystallization, the effect of DBP/DEHP ratio in diluent mixture on cross-sectional structures of membranes is shown in Fig. 5. Although the DBP ratio in diluent

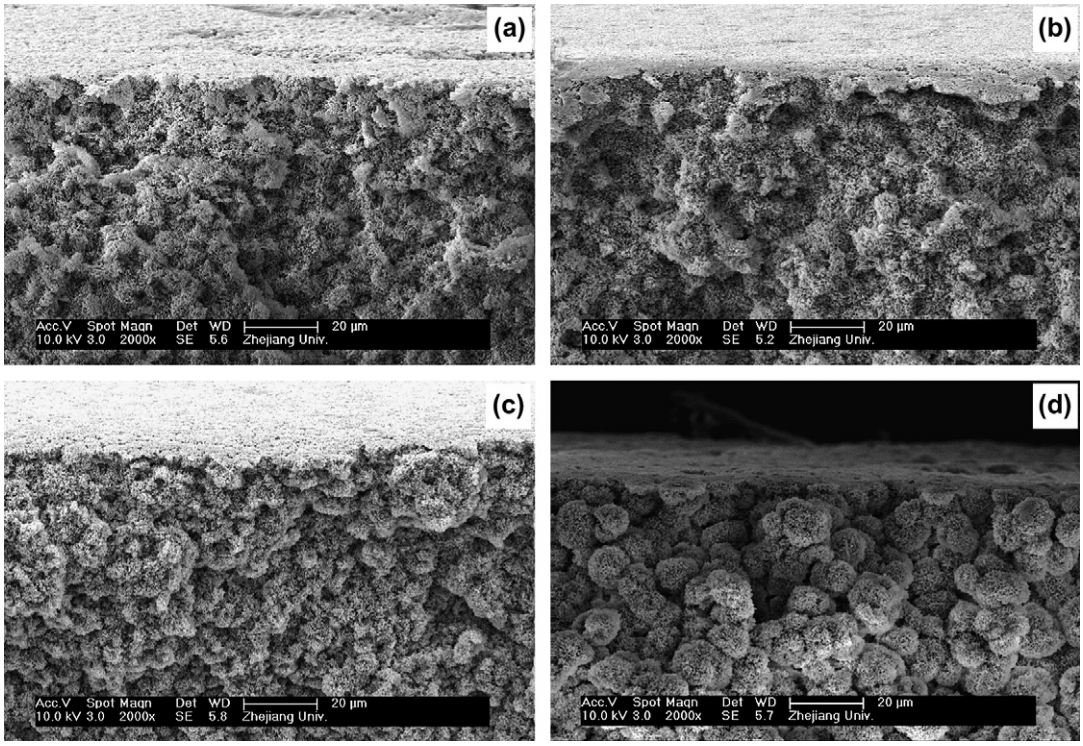

Fig. 7. SEM photographs of the cross-sections of 30 wt% PVDF membranes prepared via S–L phase separation. (a) M-d35, (b) M-d40, (c) M-d50, (d) M-d100. The bars represent 10 μm scale.

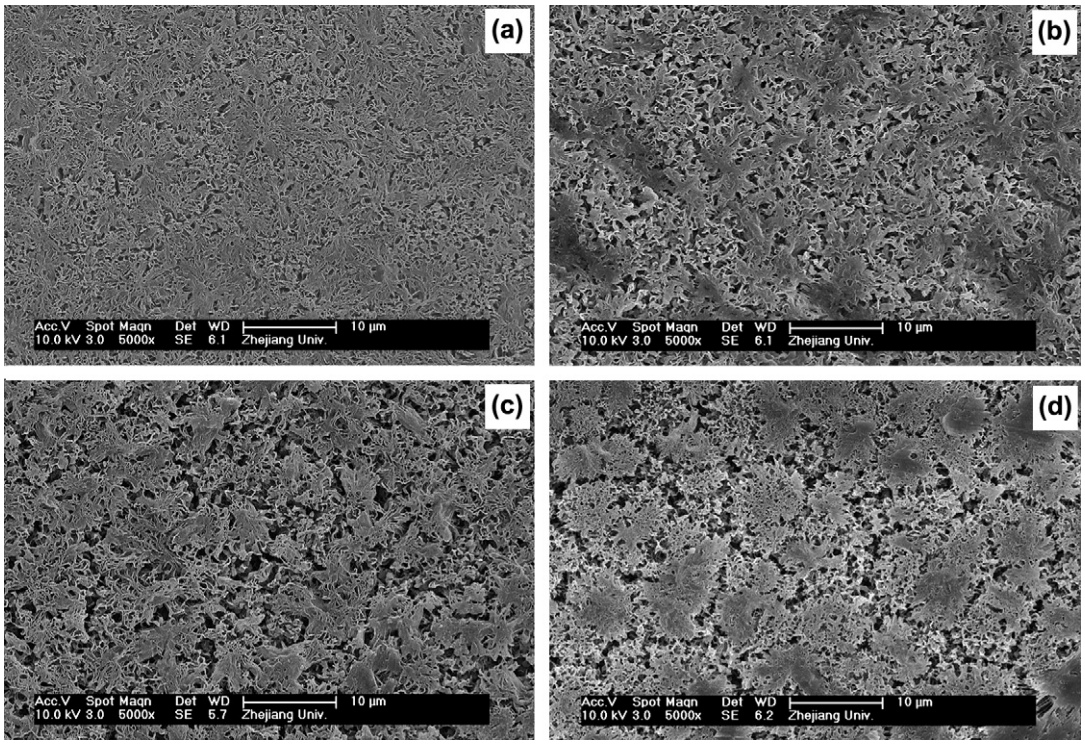

Fig. 8. SEM photographs of the surface of 30 wt% PVDF membranes prepared via S–L phase separation. (a) M-d35, (b) M-d40, (c) M-d50, (d) M-d100. The bars represent 10 μm scale.

mixture increased only slightly, four different microstructures were observed. Well connected leaf-like pores were obtained in M-d28, but larger pores were also observed as shown in Fig. 5(a). As the DBP/DEHP ratio increased to 30 wt/70 wt in diluent mixture, the corresponding membrane had a uniform sponge-like microstructure without larger pores as shown in Fig. 5(c). Although the L–L phase separation appeared in the cooling process for these samples, the structure of cellular pores, which is typical structure of membrane for system with L–L phase separation [30], was not obtained in the cross-section of membrane. Since the homogeneous mixture is quenched to the room temperature when the porous membrane is produced via TIPS process, phase separation directly enters the unstable region and proceeds through spinodal decomposition. Also the coarsening process is negligible at this condition. Thus the temperature gap between liquid–liquid phase separation temperature and the crystallization temperature of the polymer plays an important role in determining the microstructure of the porous membrane. As shown in Fig. 3, the cloud point of the sample with 28 wt/72 wt DBP/DEHP was higher than that of the sample with 30 wt/70 wt DBP/DEHP, while the crystallization temperatures of these two samples were almost the same. When the cooling condition was the same, the sample with 28 wt/72 wt DBP/DEHP had more time for L–L phase separation than that with 30 wt/70 wt DBP/DEHP. As a result, the volume fraction of lean-polymer phase was larger for the sample with 28 wt/72 wt DBP/DEHP, leading to the structure with larger pores. On the other hand, the cloud point of the sample with 32.5 wt/72.5 wt DBP/DEHP was close to its crystallization temperature as shown in Fig. 3. The L–L phase separation did not have enough time to complete before the crystallization of PVDF started to take place. A spherulitic structure was observed as shown in Fig. 5(d). Fig. 6 shows the surface structure of membranes for these four samples. Small uniform pores were obtained in M-d30 relative to other membranes.

The effect of DBP/DEHP ratio in diluent mixture on cross-sectional structures of membranes where only crystallization is observed is shown in Fig. 7. The cross-sectional structures of membranes entirely presented spherulitic structure. The spherulites become bigger and more perfect as the DBP/DEHP ratio increased in diluent mixture as shown in Fig. 7. In the case of these systems with only S–L phase separation, the viscosity of system and the interaction between polymer and diluent played two critical roles in the formation of membrane morphology. The system with higher DBP/DEHP ratio presented higher viscosity and stronger interaction between PVDF and diluent, which prevented the nucleation activity of PVDF and led to the formation of few primary nuclei at the beginning of crystallization. In the systems with the same polymer concentration, less primary nuclei had more polymer molecules to grow up. Fig. 8 shows the surface structures of membranes for these samples. Bigger pores, namely the space between spherulites, were presented as the DBP/DEHP ratio increased in diluent mixture.

3.3. The thermal and crystalline properties of porous membranes

Due to the structural difference, the DBP/DEHP ratio in diluent mixture also affects the thermal and crystalline properties

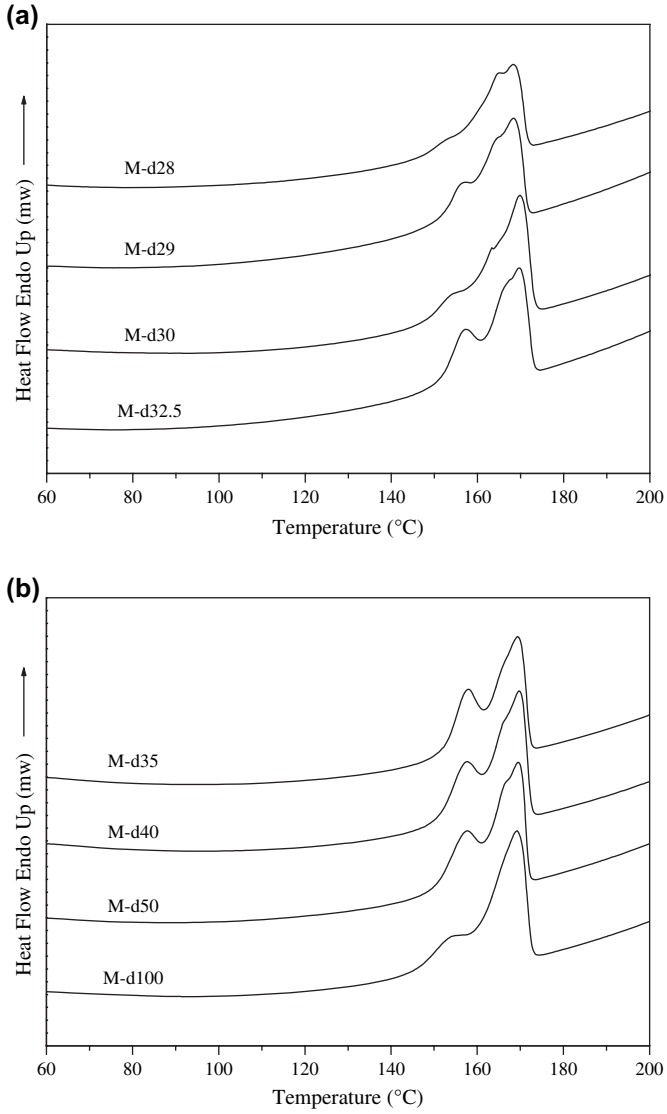

Fig. 9. DSC diagrams of the melting curves of the PVDF membranes via L–L phase separation (a) and S–L phase separation (b). Cooling rate: 10 °C/min.

of the porous membranes. Fig. 9(a) and (b) shows the DSC thermograms for PVDF porous membranes when the DBP/DEHP ratio in diluent mixture was changed. In the case of L–L phase separation observed, the melting curves of membranes reveal the presence of a ''low melting endotherm'' and a ''high melting endotherm'' as shown in Fig. 9(a). The low melting endotherm is enhanced when the sperulitic structure is presented in the M-d32.5 membrane. In the case where the S–L phase separation was observed, the low melting endotherm decreased in magnitude and shifted toward lower temperature as the DBP/DEHP ratio increased in diluent mixture, while the location of the high melting endotherm remained unaffected as shown in Fig. 9(b). The presence of the low melting endotherm was attributed to the secondary crystallization of PVDF. Secondary crystallization as a source of structural evolution has been extensively investigated by Marand and co-workers [31–33] on a variety of polymers including ethylene/octene copolymer, PEEK and polycarbonate. When the membranes presented only spherulitic structure, the existence of a secondary crystallization of PVDF

Table 2
The fusion enthalpy and crystallinity of PVDF membranes prepared with different diluent mixtures

Number	M-d28	M-d29	M-d30	M-d32.5	M-d35	M-d40	M-d50	M-d100
ΔH_f (J/g)	40.4	48.1	47.9	57.8	54.9	56.4	60.6	56.7
X_c (%)	38.6	45.9	45.8	55.2	52.5	53.9	57.9	54.2

was caused by the spherulite impingement and perfection of the internal spherulite crystallization in the later stage of crystallization process.

The fusion enthalpy and crystallinity of PVDF membranes prepared by different diluent mixture are summarized in Table 2. It was noticed that the PVDF membranes owning a spherulitic structure had higher crystallinity relative to other membranes. It can be explained that the PVDF molecules in the polymer-lean phase appearing in the process of L–L phase separation contributed to the formation of the amorphous phase of membrane.

3.4. The mechanical properties of porous membranes

Stress–strain measurements have been undertaken on dry PVDF porous membranes. Fig. 10(a) and (b) describes the

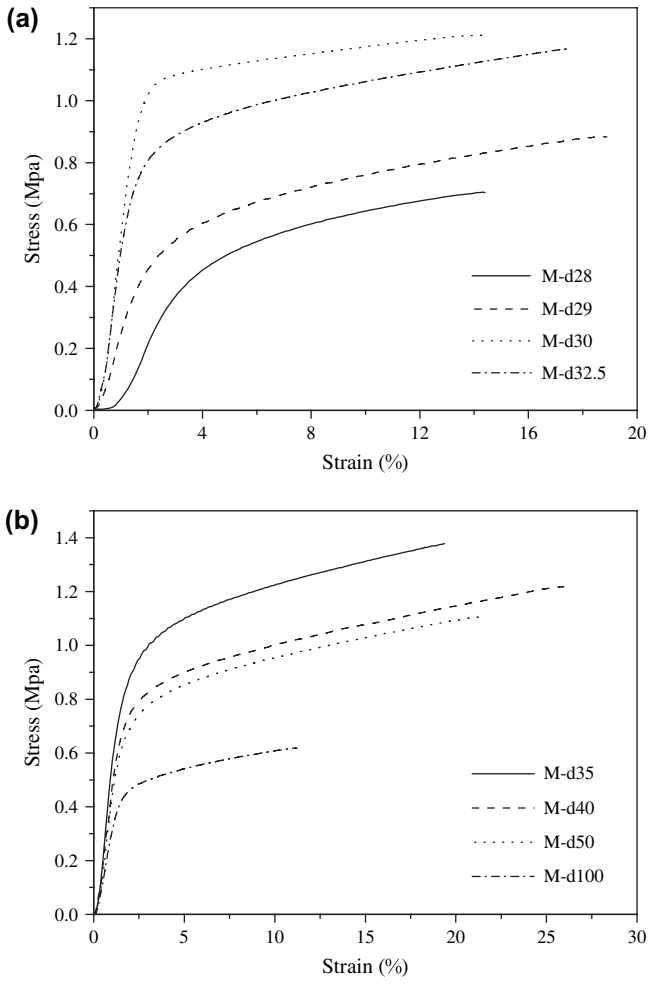

Fig. 10. Stress–strain curves of the PVDF membranes prepared via L–L phase separation (a) and S–L phase separation (b).

Table 3
Some mechanical properties of PVDF membranes prepared with different diluent mixtures

Number	M-d28	M-d29	M-d30	M-d32.5	M-d35	M-d40	M-d50	M-d100
Modulus (MPa)	21.13	34.63	62.08	52.71	62.72	58.05	53.26	42.03
Stress (MPa)	0.71	0.88	1.21	1.16	1.38	1.22	1.10	0.62
Strain (%)	14.27	18.77	14.40	17.48	19.26	25.28	21.07	11.17

stress–strain results of the membranes prepared by different diluent mixtures. Specific values of the mechanical properties of membranes are summarized in Table 3. It is found that both M-d30 and M-d35 membranes possess higher breaking stress (1.21 and 1.38 MPa) and elastic modulus (62.08 and 62.72 MPa) relative to other membranes. It is well known that the crystallinity and the microstructure of membranes play two important roles on the mechanical properties of membranes. As shown in Table 2, the crystallinity of M-d30 and M-d35 membranes was not the highest among all membranes. In other word, the higher mechanical properties of these two membranes were due to the uniform sponge-like microstructure formed via L–L phase separation for M-d30 and the closer spherulites structure formed via S–L phase separation for M-d35.

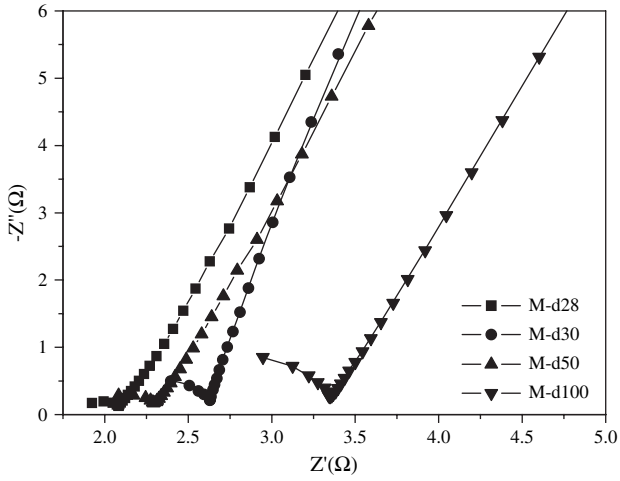

Fig. 12. The AC impedance plots at 25 °C for the polymer electrolytes made from different membranes.

3.5. The liquid electrolyte uptake of porous membranes

The liquid electrolyte uptake of membrane was defined as the weight ratio of the liquid electrolyte solution to the dry membrane. The behavior of liquid electrolyte uptake and porosity with different PVDF membranes is presented in Fig. 11. The porosity of the membranes prepared by different diluent mixtures ranged from 61.5 to 69.9%. Usually, a larger porosity leads to higher liquid electrolyte uptake of the membrane [34]. However, the change of liquid electrolyte uptake did not correlate with porosity as shown in Fig. 11. The porosity was found to be higher for M-d50 than for M-d28, but the liquid electrolyte uptake was lower for M-d50 than for M-d28. This can be due to the fact that the crystallinity of M-d50 is lower than that of M-d28, as shown in Table 2. So, it seems that the uptake of the liquid electrolyte does not depend only on the porosity of membrane but also on the crystallinity of membrane. The same result was found in the comparison of porosity and liquid electrolyte uptake between M-d30 and M-d32.5. Saito and co-workers [6] proposed that the liquid electrolyte uptake was governed by two processes. First, the liquid electrolyte filled the pores of the membrane from outside. Then, the liquid electrolyte swelled into the polymer amorphous phase to form a swollen gel. In this study, the porosity of membranes ranged in a small scale. The swelling contribution to the overall liquid electrolyte uptake that increased with the increase of the amorphous polymer phase in membrane became apparent.

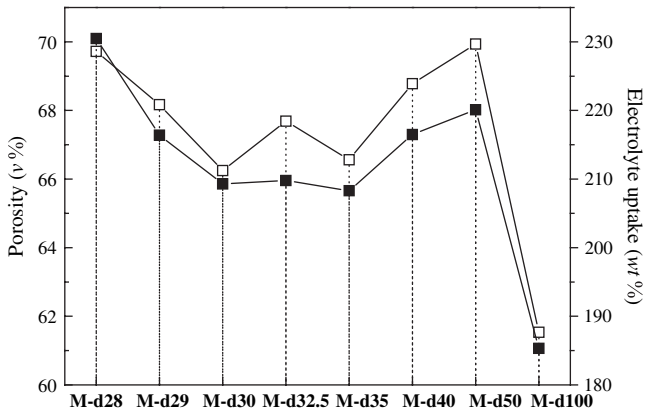

Fig. 11. Electrolyte uptake and porosity for different membranes: (■) electrolyte uptake and (□) porosity.

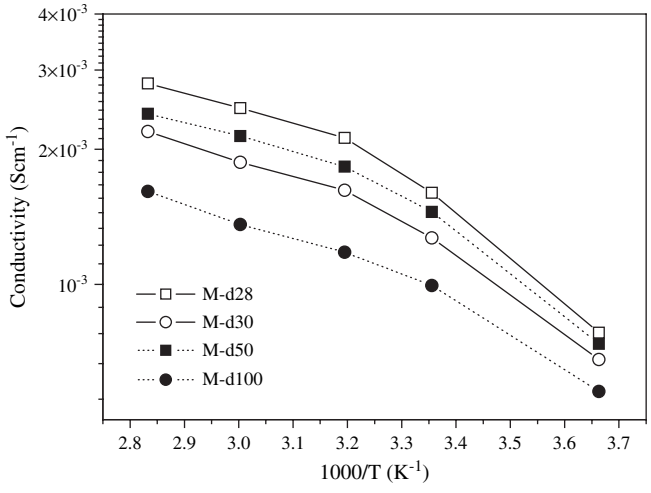

Fig. 13. Temperature dependence on ionic conductivities for the polymer electrolytes made from different membranes.

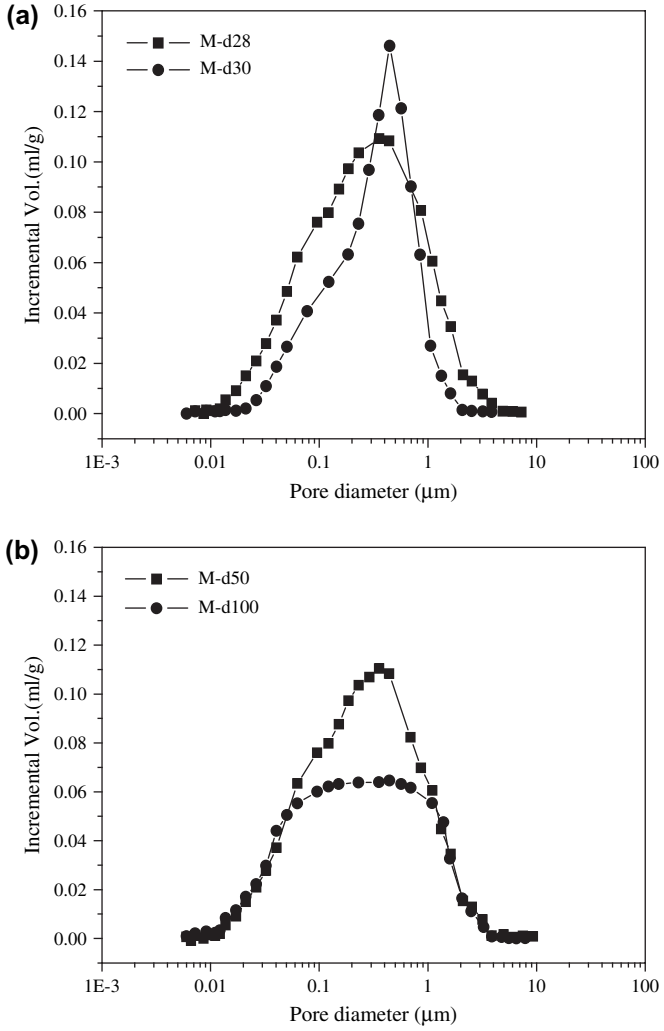

Fig. 14. Pore size distribution for the membranes prepared via L–L phase separation (a) and S–L phase separation (b).

3.6. The electrochemical properties of polymer electrolyte

The AC impedance plots at ambient temperature for four polymer electrolytes based on the membranes of different microstructures, as the leaf-like for M-d28, sponge-like for M-d30, small spherulites for M-d50 and big spherulites for M-d100, are shown in Fig. 12. The bulk resistance (R_b) was measured from the high frequency intercept on the real axis. Fig. 13 shows the ionic conductivities obtained from AC impedance spectrums for these polymer electrolytes at various temperatures. Most of the polymer electrolytes presented ambient temperature conductivities of greater than 10^{-3} S/cm. The ionic conductivities for the polymer electrolytes based on M-d28 and M-d50 were higher than that for the polymer electrolytes based on M-d30 and M-d100 at various temperatures, which accorded with the higher electrolyte uptake of M-d28 and M-d50.

Generally, ion conductivity is governed by the content of carrier ions and their mobility. A mechanism for the ionic conduction in the polymer electrolytes along two conduction

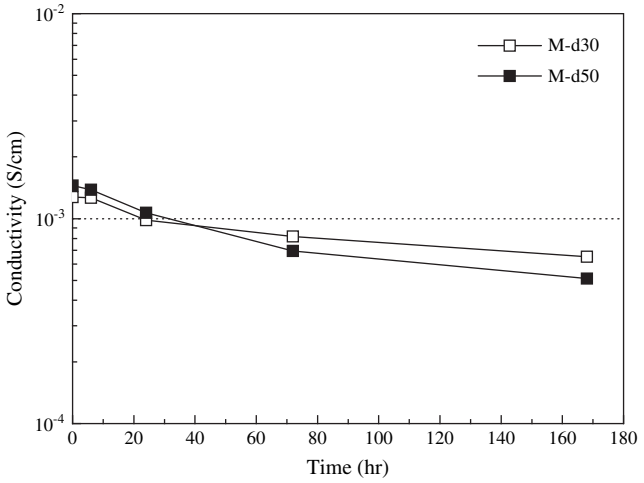

Fig. 15. Time evolution of the conductivity for the polymer electrolytes made from M-d30 and M-d50 at 25 °C.

paths has been postulated [35–37]. Two conduction paths consist of a swollen polymer phase of lower conductivity and a liquid electrolyte phase of higher ionic conductivity. The liquid electrolyte phase, which fills the pore of the membrane, can be regarded as a major conducting channel. The polymer electrolytes prepared with M-d28 and M-d50 exhibit higher ionic conductivities, which can be well explained by this two-phase model. The pore size distributions measured by the mercury intrusion method are reported in Fig. 14 for M-d28, M-d30, M-d50 and M-d100. Higher porosities for M-d28 and M-d50 relative to M-d30 and M-d100 were observed in Fig. 14. On the other hand, for M-d28 and M-d50, pores larger than 1 μm in a wide pore size distribution are observed while for M-d30, a peak around 0.45 μm in a narrow pore size distribution is observed. The increase of porosity and pore size for M-d28 and M-d50 leads to the increase of the liquid electrolyte phase in pores which enhanced the conductivity of polymer electrolyte accordingly.

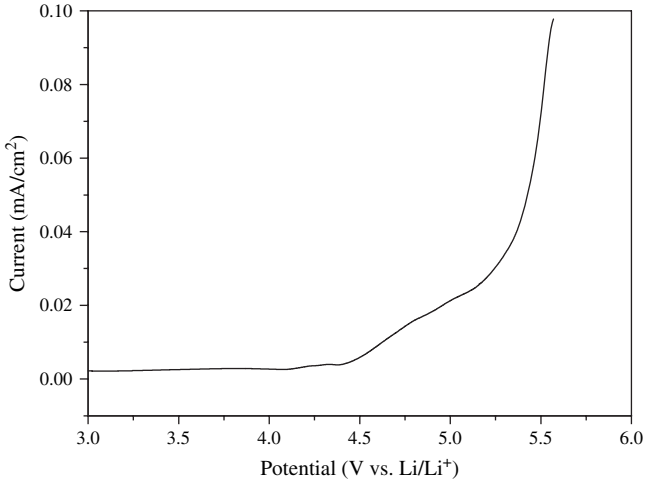

Fig. 16. Current–voltage curve of a Li/polymer electrolyte/SS cell at 25 °C (sweep rate: 5 mv/s and SS: stainless steel). The polymer electrolyte made from M-d30.

Fig. 15 illustrates the time dependence of the ionic conductivity for two polymer electrolytes based on M-d30 and M-d50. It can clearly be seen that the conductivity for the polymer electrolyte based on M-d30 decreases more slowly with time than that for the polymer electrolyte based on M-d50. The difference in the ionic conduction behavior with time is believed to be due to the change of the quantity of electrolyte in the membrane, which results from liquid electrolyte leakage. Since the crystallinity of M-d30 was relatively low, more liquid electrolytes swelled in the amorphous phase which contributed to retain electrolytes. On the other hand, it is also due to the differences in the pore dimensions. In the M-d30, in fact, the pores are relatively small and a ''good'' spatial continuity exists between the pores; therefore, it is reasonable to imagine that the swelling of the amorphous phase will take place facilely. In contrast, the spaces between spherulites of M-d50 are larger and the contact between amorphous phase and liquid electrolyte is worse which slackens the swelling process.

The electrochemical stability of the polymer electrolyte based on M-d30 was evaluated by linear sweep voltammetry as shown in Fig. 16. As one can see, no decomposition of any component takes place below 4.5 V (vs Li^+/Li), which is acceptable for high voltage cathode materials.

4. Conclusions

Preparation of PVDF porous membrane via the thermally induced phase separation TIPS process using diluent mixtures of DBP and DEHP, a method to fabricate the microporous matrix of polymer electrolyte for lithium ion battery, has been shown to easily produce membranes with various microstructures by only varying the DBP/DEHP ratio in diluent mixture. With the assistance of phase diagram, the effects of the DBP/DEHP ratio in diluent mixture on the microstructure of membrane were investigated. The phase behaviors of a ternary mixture of PVDF/DBP/DEHP were determined to control systematically L–L phase separation and S–L phase separation by changing the DBP/DEHP ratio in diluent mixture. In the case of L–L phase separation, the evolution of membrane microstructures, ranging in well connected leaf-like, uniform sponge-like and spherulitic microstructures, was due to the temperature gap between liquid–liquid phase separation temperature and crystallization temperature. On the other hand, the microstructures of membranes prepared via S–L phase separation showed only spherulitic structures and the size of spherulites increased with the increase in DBP/DEHP ratio. The relationship between the performance of membrane, the electrochemical property of polymer electrolyte and the final microstructure was also investigated. It was found that the membrane with uniform sponge-like microstructure possessed higher elastic modulus and stress than most membranes and the polymer electrolyte prepared from that had an ambient temperature conductivity of 1.3×10^{-3} S/cm. Also this polymer electrolyte exhibited a good reservation of liquid electrolyte and a wide electrochemical stability up to 4.5 V vs Li^+/Li.

Acknowledgements

This work was supported by the National Basic Research Program of China (no. 2003CB615705) and National Nature Science Foundation (no. 50433010).

References

[1] Jiang Z, Carroll B, Abraham KM. Electrochim Acta 1997;42:2667–77.
[2] Periasamy P, Tatsumi K, Shikano M, Fujieda T, Sakai T, Saito Y, Mizuhata M, Kajinami A, Deki S. Solid State Ionics 1999;126:285–92.
[3] Muniyandi N, Kalaiselvi N, Periyasamy P, Thirunakaran R, Ramesh babu B, Gopukumar S, et al. J Power Sources 2001;96:14–9.
[4] Gozdz AS, Schmutz CN, Tarascon JM, Warren PC. US Patent 5,540,741 1997.
[5] Boudin F, Andrieu X, Jehoulet C, Olsen II. J Power Sources 1999;81–82:804–7.
[6] Kataoka H, Saito Y, Sakai T. J Phys Chem B 2000;104:11460–4.
[7] Michot T, Nishimoto A, Watanabe M. Eletrochim Acta 2000;45:1347–60.
[8] Magistris A, Mustarelli P, Parazzoli F, Quartarone E, Paiggio P, Bottino A. J Power Sources 2001;97–98:657–60.
[9] Hiatt WC, Vitzthum GH, Wagener KB, Gerlach K, Wagener KB, Josefiak C. ACS Symposium Series, vol. 269, Washington, DC; 1985. p. 229–44.
[10] Su Y, Chen CX, Li YG, Li JD. J Macromol Sci A 2007;44:99–104.
[11] Li XF, Lu XL. J Appl Polym Sci 2006;101:2944–52.
[12] Smith SD, Shipman GH, Floyd RM, Freemyer HT, Hamrock SJ, Yandrasits MA, et al. WO Patent 035, 641; 2005.
[13] Gu M, Zhang J, Wang X, Tao H, Ge L. Desalination 2006;192:160–7.
[14] Lloyd DR, Kim SS, Kinzer KE. J Membr Sci 1990;52:239–61.
[15] Matsuyama H, Okafuji H, Maki T, Teramoto M, Kubota N. J Membr Sci 2003;223:119–26.
[16] Hellman DJ, Geenberg AR, Krantz WB. J Membr Sci 2004;230:99–109.
[17] Matsuyama H, Takida Y, Maki T, Teramoto M. Polymer 2002;43:5243–8.
[18] Shang M, Matsuyama H, Teramoto M, Okuno J, Lloyd DR, Kubota N. J Appl Polym Sci 2005;95:219–25.
[19] Hua FJ, Park TG, Lee DS. Polymer 2003;44:1911–20.
[20] Kim LU, Kim CK. J Polym Sci Part B Polym Phys 2006;44:2025–34.
[21] Vadalia HC, Lee HK, Myerson AS, Levon K. J Membr Sci 1994;89:37–50.
[22] Brandrup J, Immergut EH, Grulke EA. Polymer handbook. 4th ed. New York: Wiley; 1999. p. VII675–711.
[23] Nakagawa K, Ishida Y. J Polym Sci Polym Phys Ed 1973;11:2153–71.
[24] Cao JH, Zhu BK, Xu YY. J Membr Sci 2006;281:446–53.
[25] Liu B, Du Q, Yang Y. J Membr Sci 2000;180:81–92.
[26] van de Witte P, Dijkstra PJ, van den Berg JWA, Feijen J. J Membr Sci 1996;117:1–31.
[27] Song SW, Torkelson JM. Macromolecules 1994;27:6389–97.
[28] Burghardt WR. Macromolecules 1989;22:2482–6.
[29] Matsuyama H, Iwatani T, Kitamura Y, Tearamoto M, Sugoh N. J Appl Polym Sci 2001;79:2449–55.
[30] Matsuyama H, Berghmans S, Lloyd DR. Polymer 1999;40:2289–301.
[31] Alizadeh A, Richardson L, Xu J, McCartney S, Marand H, Cheung YW, Chum S. Macromolecules 1999;32:6221–35.
[32] Marand H, Alizadeh A, Farmer R, Desai R, Velikov V. Macromolecules 2000;33:3392–403.
[33] Alizadeh A, Sohn S, Quinn J, Marand H, Shank LC, Darrell Iler H. Macromolecules 2001;34:4066–78.
[34] Song JY, Cheng CL, Wang YY, Wan CC. J Electrochem Soc 2002;149:A1230–6.
[35] Capiglia C, Saito Y, Yamamoto H, Kageyama H, Mustarelli P. Electrochim Acta 2000;45:1341–5.
[36] Bohnke O, Frand G, Rezrazi M, Rousselot C, Truche C. Solid State Ionics 1993;66:97–104.
[37] Bohnke O, Frand G, Rezrazi M, Rousselot C, Truche C. Solid State Ionics 1993;66:105–12.